International Journal of Heat and Mass Transfer 52 (2009) 3456–3463

Contents lists available at ScienceDirect

International Journal of Heat and Mass Transfer

journal homepage: www.elsevier.com/locate/ijhmt

Modeling and testing of an advanced compact two-phase cooler for electronics cooling

Mark Aaron Chan, Christopher R. Yap, Kim Choon Ng *

Department of Mechanical Engineering, National University of Singapore, 10 Kent Ridge Crescent, Singapore 119260, Singapore

ARTICLE INFO

Article history:
Received 6 October 2008
Received in revised form 13 February 2009
Accepted 13 February 2009
Available online 16 April 2009

Keywords:
CPU cooling
Enhanced nucleate boiling
Porous media
Heat sinks

ABSTRACT

This paper describes the modeling, design, and testing of a high flux and yet compact two-phase CPU cooler, with excellent attributes of low thermal resistance that are derived from the intrinsic design features of phase change phenomena and minimal vapor pressure drop of the device. For the same footprint of a conventional cooler, the prototype rejects more than twice the capacity of CPUs of today. The unique design minimizes its overall size and yet provides adequate area for forced convection cooling. Testing was conducted over an assorted heat loads and air flow rates flowing through the fins, achieving a best performance of 0.206 K/W of device thermal resistance at a rating of 203 W under an air flow rate of 0.98 m^3/min. The prototype device is orientation free where a 90° tilt could perform at the same rating conditions.

© 2009 Elsevier Ltd. All rights reserved.

1. Introduction

The advent of multi-core processors coupled with higher clock rates of CPUs has presented a great challenge for the design of high flux coolers of computers, particularly when the coolers are constrained to have the footprint of a single assembly. When clock rate goes beyond 3.6 GHz, conventional coolers available today tend to exceed the thermal design limits (TDL), a thermal barrier yet to be solved, as shown in Fig. 1. This provides the motivation for this study which contributes high heat-flux transfer solutions for high performance CPUs. CPU cooling markets today are categorized into the following: conventional air-cooled fin heat sinks, liquid cooling with remote ambient air-cooled heat sink or radiator, and miniature heat pipes with air-cooled condenser remotely located or directly situated on the CPU. Inherent short comings of current CPU cooling devices are summarized as follows:

(i) Significant heat spreading resistance is encountered by fin-fan air cooling arising from a small source area (typically 1 cm^2) to a larger fin base plate, creating greater temperature non-uniformity. The experiment and numerical simulations by Siani and Webb [1] show that such cooling devices can only handle heat loads up to 100 W from a 2.56 cm^2 CPU case area.
(ii) Liquid cooling for high heat flux applications have poor heat spreading resistance of base plate, and a larger liquid contact area is needed to counter its mediocre single-phase convective heat transfer. It usually has a bulky ambient air-cooled heat sink and a high pressure miniature pump. Experimental results of micro-channel heat exchangers for liquid cooling applications, such as the study from Chang et al. [2], albeit having good performance with an overall thermal resistance of 0.23 K/W from a 1 cm^2 heat source, such cooling device needed a large air-cooled radiator of 120 mm and a miniature pump of 10 kPa back pressure.
(iii) Miniature heat pipe array, although proven reliable and can removed heat effectively from source to air-cooled surfaces at various orientations, heat pipe coolers are generally bulkier. The experimental results of Moon et al. [3] and Kim et al. [4] indicate that heat pipes have an overall resistance ranging from 0.35 to 1.0 K/W. Remote locations of condensers from evaporator in loop heat pipes are possible due to the minimal hydraulic resistance from its smooth vapor and liquid lines, while evaporator wicks are used to facilitate liquid return. The test results of Maydanik et al. [5] and Singh et al. [6] indicate thermal resistance typically ranges from 0.58 K/W to 1.2 K/W.

This paper presents a compact two-phase CPU cooler that has attributes to overcome the above-mentioned short comings, and it has high heat fluxes for heat removal and has orientation free features.

2. Mathematical modeling

The proposed device, as described in the patent of Ng et al. [7], has three major but integrated sections viz. an evaporator,

* Corresponding author. Tel.: +65 65162214; fax: +65 67791459.
E-mail address: mpengkc@nus.edu.sg (K.C. Ng).

0017-9310/$ - see front matter © 2009 Elsevier Ltd. All rights reserved.
doi:10.1016/j.ijheatmasstransfer.2009.02.044

Nomenclature

A	area (m^2)
Cp	specific heat capacity (J/K kg)
D_h	hydraulic diameter (m)
f_{app}	friction factor
g	gravitational acceleration (m/s^2)
H	fin height (m)
h	heat transfer coefficient (W/m^2 K)
h_{fg}	latent heat of vaporization (kJ/kg)
K_c	contraction loss coefficient
K_e	exit loss coefficient
K	thermal conductivity (W/m K)
L	fin channel flow length (m)
l	thickness (m)
NB	number of fin base
NF	number of fins
N_{seg}	number of symmetrical segments
Nu	Nusselt number
NTU	number of transfer unit
P	pressure (Pa)
Pm	fin perimeter (m)
Pr	Prantl number
q	heat loss (W)
q''	heat flux (W/m^2)
R	thermal resistance (W/K)
Re	Reynolds number
T	temperature (K)
V	velocity (m/s)
s	fin gap (m)

Greek

ε	effectiveness
μ	viscosity (kg/m s)
ρ	density (kg/m^3)
σ	surface tension (N/m)

Subscript

atm	atmosphere
ave	average
b	boiling
cd	cooling device
cs	fin cross section
chan	channel
cond	condensation
conv	convection
f	liquid
fin	fin
g	vapor
int	interface
n	fin indication
o	ambient air
p	device bottom plate
s	heat source
sp	spreading
superheat	boiling superheat
w	wetted porous media

condenser and an array of air-cooled curvilinear fins, as shown in Fig. 2. The evaporator (copper) has a liquid-filled porous structure for boiling enhancement which takes in heat from the CPU case through a thermal interface material (thermal grease). At low vacuum pressures, the heat from CPU boils a liquid in the evaporator and the latent mode ensures high heat flux via the heat of the vaporization. The generated vapor condenses on the adjacent wall of the tube sections which operates as a condenser, utilizing the high film-wise condensation flux to give a uniform temperature distribution. Heat is rejected into the fins which are then cooled by the convective air. Condensate can be transported back into the evaporator section by, firstly, the gravity flow due to its upright orientation and secondly, by capillary action from the porous structure inside the evaporator, giving a continuous supply of coolant for evaporation at the base. The evaporator may be placed in an inverted position with the liquid bulk in contact with the said structure. The compactness of the device is attained through the integration of evaporator and condenser sections into a tube section and working the condensable fluid at its saturated properties. Table 1 shows the detailed dimensions of the device.

3. Governing equations

For direct mounting onto the CPU, a thermal paste is used at the contact surface and this interface resistance between the CPU and the cooling device's base plate is given by

$$R_{\text{int}} = \frac{l_{\text{int}}}{k_{\text{int}} A_{\text{int}}} \tag{1}$$

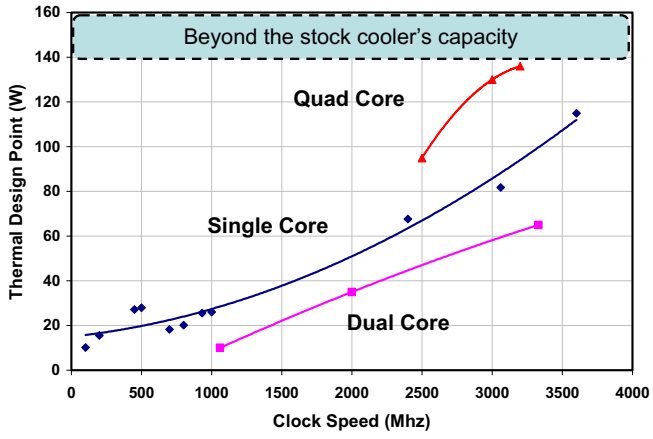

Fig. 1. Evolution of thermal heat generation (W) versus the clock speeds of CPUs.

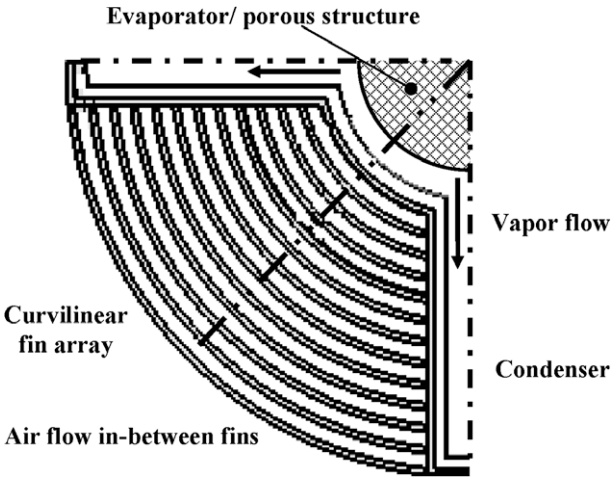

Fig. 2. Top section view of the two-phase cooler.

Table 1
Dimensions of two-phase cooler.

Evaporator base area	7 cm^2
Evaporator base thickness	4.5 mm
No. of condensers	4
Total condenser area	96 cm^2
Fins/condenser	10
Fin thickness	1 mm
Fin pitch	2 mm
Fin length	40 mm
Total fin area	1443.4 cm^2
Total convective heat transfer area	1554.0 cm^2

Heat spreading due to the device's base area being larger than the CPU's encapsulation area can be given by an approximate formula provided by Lee et al. [8]:

$$R_{sp} = \frac{\sqrt{A_p} - \sqrt{A_s}}{k_p\sqrt{\pi A_p A_s}}\left(\frac{\lambda k_p A_p R_{cd} + \tanh(\lambda l_p)}{1 + \lambda k_p A_p R_{cd}\tanh(\lambda l_p)}\right) \tag{2}$$

where $\lambda = \frac{\pi^{3/2}}{\sqrt{A_p}} + \frac{1}{\sqrt{A_s}}$; and $R_{cd} = R_p + R_b + R_{cond} + R_{conv}$. The device's base-plate thickness contributes a thermal resistance given by:

$$R_p = \frac{l_p}{k_p A_p} \tag{3}$$

A porous structure is bonded to the device's base plate as a technique to enhanced boiling. A modified Rohsenhow correlation for pool boiling on porous structures at sub-atmospheric conditions provided by Ng et al. [9], which predicts the boiling superheat required for a certain heat flux at various pressure conditions and boiling enhancements. The exponent α has a negative sign implying a decreasing temperature superheat as wetted heat transfer area is increased. The boiling resistance can be calculated subsequently.

$$\Delta T_{superheat} = \left(\frac{C_{sf} h_{fg} \mathrm{Pr}_f^s}{C_{pf}}\right)\left[\frac{q''}{\mu_f h_{fg}}\left(\sqrt{\frac{\sigma}{g(\rho_f - \rho_g)}}\right)\right]^l \left(\frac{P}{P_{atm}}\right)^m \left(\frac{A_{wetted}}{A_{base}}\right)^\alpha \tag{4}$$

$$R_b = \frac{\Delta T_{superheat}}{q_{cooling}} \tag{5}$$

where $C_{sf} = 0.132$, $l = 0.33$, $m = 0.293$, and $\alpha = -0.0984$.

Falling film condensation is expected on the vertical sides of the condenser section. An empirical correlation by Nusselt [10] from Holman [11] was used to predict the heat transfer coefficient of the said condenser section, condensation resistance is calculated subsequently:

$$h_{cond} = 0.934\left[\frac{\rho_f(\rho_f - \rho_g) g h_{fg} k_f^3}{\mu_f (T_{sat} - T_{cond}) L_{cond}}\right]^{1/4} \tag{6}$$

$$R_{cond} = \frac{1}{h_{cond} A_{cond}} \tag{7}$$

Air flowing externally through an array of curvilinear channels was approximated to be parallel plate channels and the configuration permits the use the friction factor data for a developing laminar flow through parallel plates as cited by Shah and London [12] and is fitted by Siani and Webb [1] in the form:

$$f_{app}\mathrm{Re} = B + \frac{W(D_h \mathrm{Re})}{L} \tag{8}$$

where $B = 23.73$, $W = 0.2198$, which have been regressed from the data.

The inlet loss coefficient K_c for flow into rectangular duct with small aspect ratio (Fin gap/Fin height) is taken from Idelchik [13]. A curve fit for the exit loss coefficient K_e for parallel plates is taken from Copeland [14], the data was gathered by Kays and London [15]

$$K_c = 0.45 \tag{9}$$

$$K_e = (1 - \sigma^n)^2 - 0.4\sigma^n \tag{10}$$

where σ is the area contraction ratio (fan free flow area/heat sink flow area).

Then the total channel pressure drop for each channel is given by the sum of the inlet, friction, and exit losses. Solving this requires successive iteration of the channel velocity V_{chan}^n such that pressure drop across every channel is the same and that the total air flow rate of the heat sink must be equal to the available fan air flow rate for that pressure (balance point in the fan curve Fig. 9a).

$$\Delta P_{chan}^n = \left(K_c + 4f_{app}^n x^+ + K_e^n\right)\left(\rho_o V_{chan}^{2\ n}\right)/2 \tag{11}$$

Finally, the convective heat transfer of a laminar developing flow in a rectangular channel was studied by Shah and London [12] and the data was curve fitted by Siani and Webb [1] into the equation below:

$$Nu_{ave}^n = X + \frac{Y(D_h \mathrm{RePr})}{L} - Z\left(\frac{s}{H_f}\right) \tag{12}$$

where $X = 7.43$, $Y = 0.0405$, $Z = 13.12$, which have been regressed from the data.

With the convective heat transfer coefficient known, the following equation for heat losses though each fin and base can be solved; subsequently this was summed to get the total convective heat transfer resistance of the air-cooled. Each of the summed term

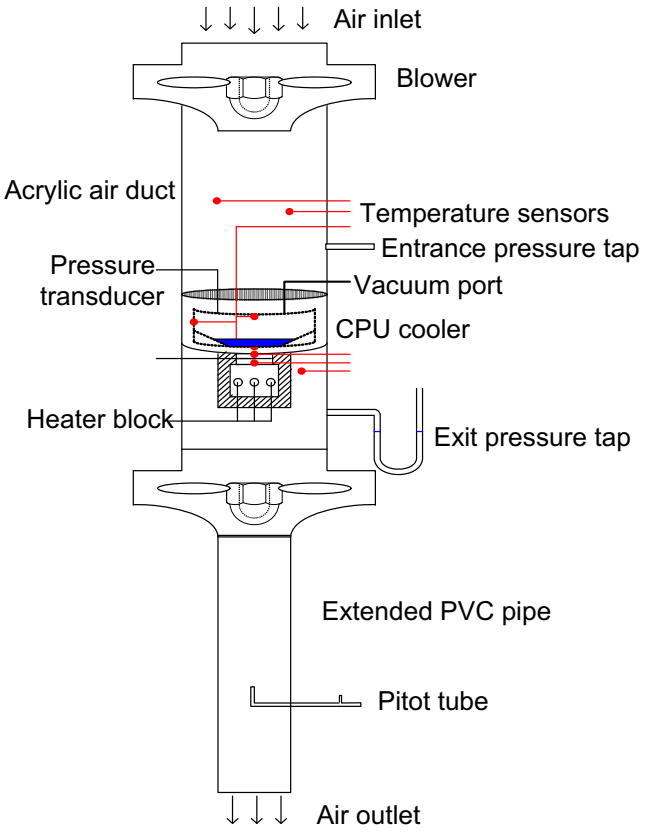

Fig. 3. Schematic of the testing rig.

is multiplied by N_{seg} because the model is $1/N_{seg}$ of the whole device.

$$q^n_{fin} = \varepsilon^n \sqrt{h^n_{fin} P m^n k^n_{fin} A^n_{cs}} (T_{cond} - T_o) \tanh(m^n H)/NTU^n \quad (13)$$

$$q^n_{base} = \varepsilon^n h^n_{fin} A_{base} (T_{cond} - T_o)/NTU^n \quad (14)$$

$$R_{conv} = \frac{(T_{cond} - T_\infty)}{N_{seg} \times \Sigma_1^{NF} q^n_{fin} + N_{seg} \times \Sigma_1^{NB} q^n_b} \quad (15)$$

where $m = \sqrt{\frac{h^n_{fin} P m^n}{k^n_{fin} A^n_{cs}}}$

All of the said governing equations are solved simultaneously using mathematical solver, with variable water and air properties.

4. Experimental apparatus and procedure

The schematic and pictorial views of the experimental apparatus used to measure the performance of the designed CPU cooler are shown in Figs. 3 and 4, respectively. The apparatus integrates a flow bench and a thermal tester into one single set-up, this enables the simultaneous measurement of thermal resistances in the device for various air flow rates and heat loads. Air flow was controlled by two variable transformers of centrifugal blowers located at the inlet (pushing) and outlet (pulling) of air flowing in a duct. It maintains the air pressure in between the CPU cooler to be at atmospheric conditions which is crucial for correct heat transfer analysis and is similar to the state when the cooler operates in the ambient conditions. Heat load is introduced to the cooling device through an insulated 3 cm diameter copper heater block (with three 150 W cartridge heater inserts) clamped onto its bottom plate. The porous structure in the cooler's evaporator is made from commercially available 60 pores per linear inch (PPI) copper metal foam (Porvair). It has a pore diameter of 0.38 mm, 95% porosity, and provides approximately 4000 square meter of surface area per cubic meter.

Static pressure taps are located at the entrance and exit section of the cooling device that measure the pressure drop across it.

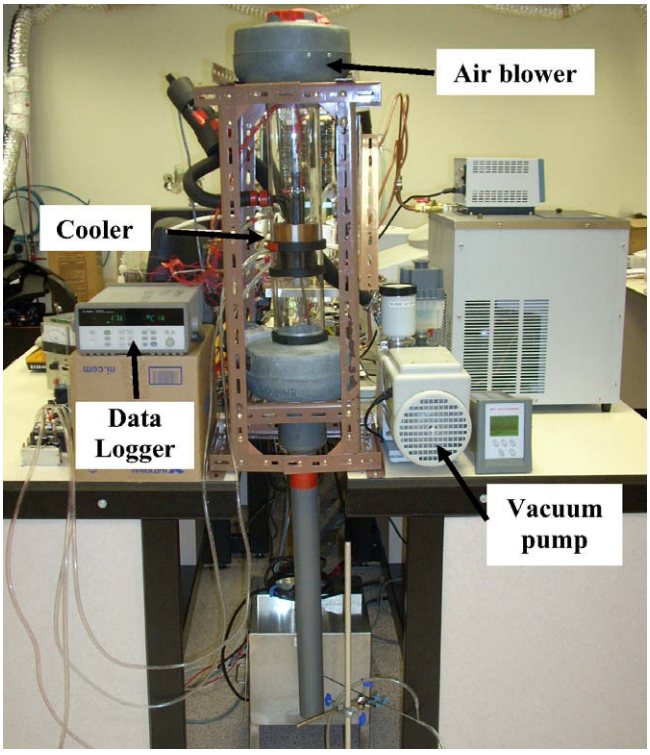

Fig. 4. Pictorial view of the testing rig.

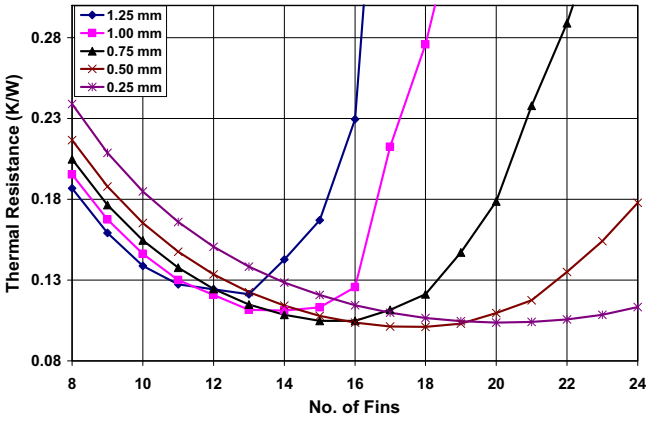

Fig. 5. Convection thermal resistance of the cooler versus number of fins for various fin configurations.

Pitot-tube was placed at the extended outlet of the air duct measuring the air flow rate. Two low pressure differential transmitters (type Johnson Controls DPT 2641-1) are used to measure the pressure drop and the air velocity from the pitot tube. Thermistors having an accuracy of ±0.1 °C are used to measure the corresponding temperature levels on each section of the device, namely the bottom plate, boiling surface, saturation temperature, and condenser

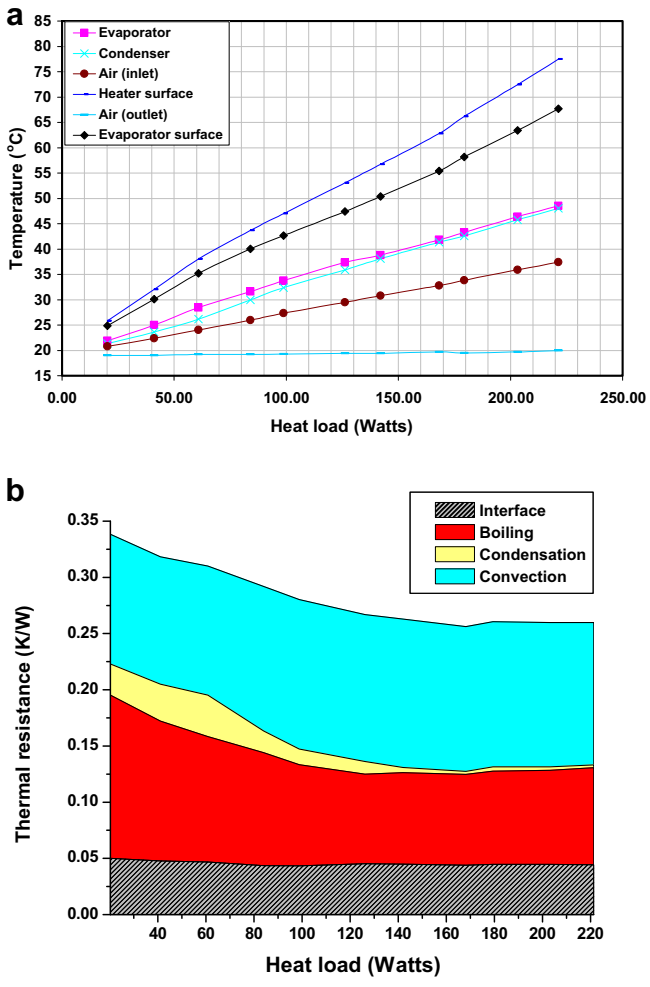

Fig. 6. (a) Steady state temperature levels at various heat loads (vertical orientation). (b) Thermal resistances at various heat loads (vertical orientation).

wall surface. RTDs having ±0.3 °C accuracy are used to measure temperatures at the heater surface and air inlet and outlet. Temperature readings are then logged by a HP Agilent 34970A data logger. A BOC Edwards ASG 1000 mbar vacuum pressure sensor is used to monitor the saturation pressure of water.

Heat leak tests were done on the insulated heater block to account for radiation and convection heat losses. For this test, the heater block is not in contact with the cooler such that all the heat input is completely leaked to the ambient. Electrical power input to the heater was varied from 1 to 10 W in steps of 0.5 W, the heater block would then reach a certain steady temperature above the ambient for every electrical power input, and that electrical power is taken to be the heat leak value at this temperature difference between the heater block and the ambient air. This was done at various air flows covering the testing range. The definition of heat load hereafter shall be the net heat load (electrical power input minus the calibrated heat leak).

The testing commences with the charging of the working fluid (water) into the device, a rotary vane vacuum pump purges air and non-condensible gases out of the system. Blowers are then turned on and varied to the desired air flow rate with the air pressure in the test section maintained at 1 atmosphere, as is in the actual case. Then the electrical power input to the cartridge heaters is varied in steps from 20 W to 220 W, steady state temperatures at each heat load is used to compute for various thermal resistances in the device.

5. Results and discussion

Majority of CPU coolers incur more than 50% of their thermal resistance due to air convection, which is why it is known to be the major "bottleneck" of such devices. Knowing the importance of the air side cooling, optimization of the curvilinear fin array was done for various fin thickness as shown in Fig. 5. The chart shows that at larger fin pitches or lower number of fins (i.e. 11 and below), thermal resistance is inversely proportional to fin thickness. The optimal fin configuration found has a fin thickness of 0.5 mm and a pitch of 1.66 mm with the lowest convection thermal resistance of only 0.1011 K/W. Unfortunately, this fin is too thin to cut mechanically. Subsequently, a fin thickness of 1 mm and 2 mm pitch is fabricated.

Steady state temperatures for all components of the cooling device is plotted against the heat load at a fan flow rate of 0.98 m^3/min (balance point) shown in Fig. 6a. The performance of the cooling device was impressive, operating below the TDL (heater surface temperature did not exceed 75 °C) even with 200 W of heating. In terms of thermal resistances, Fig. 6b shows us a clear overview of the four major resistances of the device. At lower heat loads of 20 W to 100 W, the evaporator has low evaporator saturation temperatures of 20 °C to 35 °C, both the condensation and boiling resistances are larger. At high heat loads, both resistances decrease asymptotically. This phenomenon was expected for water boiling at very low saturation pressures (2–4 kPa) as it requires higher boiling superheat, as explained by McGillis et al. [16] and Gorenflo [17]. The reason for the asymptotic reduction in thermal resistance could be reinforced by pictorial evidence from high speed photography, as shown with graphs of Fig. 7a and b: The two sequences of monochrome pictures depict the nucleation, formation, interaction, and departure of bubbles on a porous metal-claded boiling surface were captured under saturation pressures of 2 kPa and 9 kPa at a supplied heat flux of 5 W/cm^2. The difference between the two ebullition processes is distinct and observable. For the case of 2 kPa, few active nucleation sites are found while the bubble-departure frequency (e.g. one bubble per 400–500 ms) is lesser, implying that boiling could not be sustained despite the many boiling sites provided by the foam metal. Whereas, for the 9 kPa case,

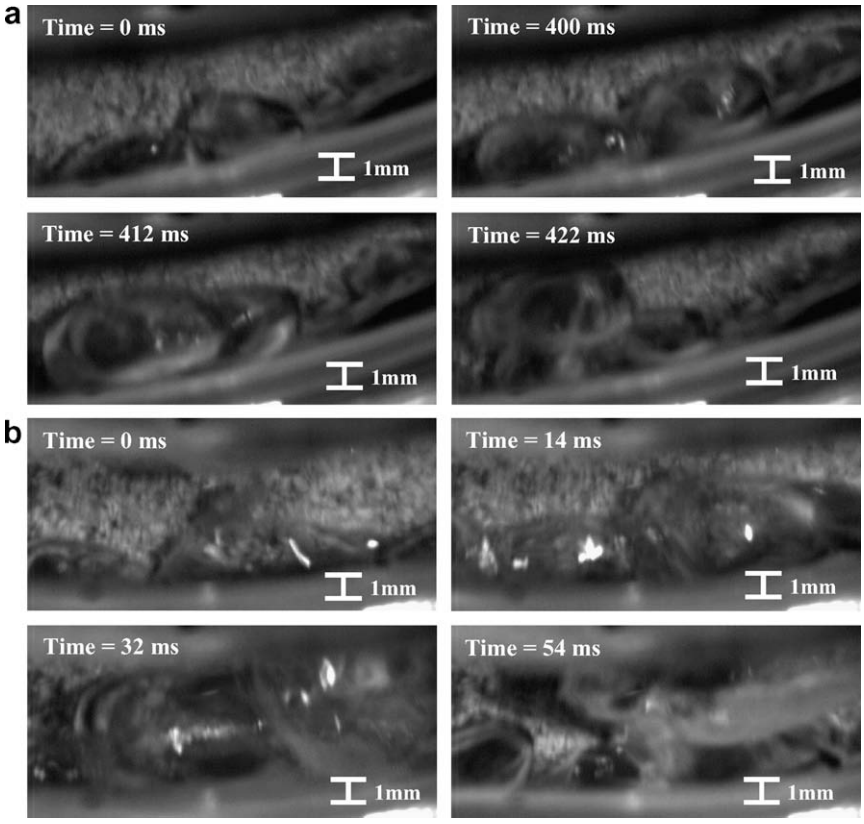

Fig. 7. (a) High speed video of water boiling from a porous structure at 2 kPa. (b) High speed video of water boiling from a porous structure at 9 kPa.

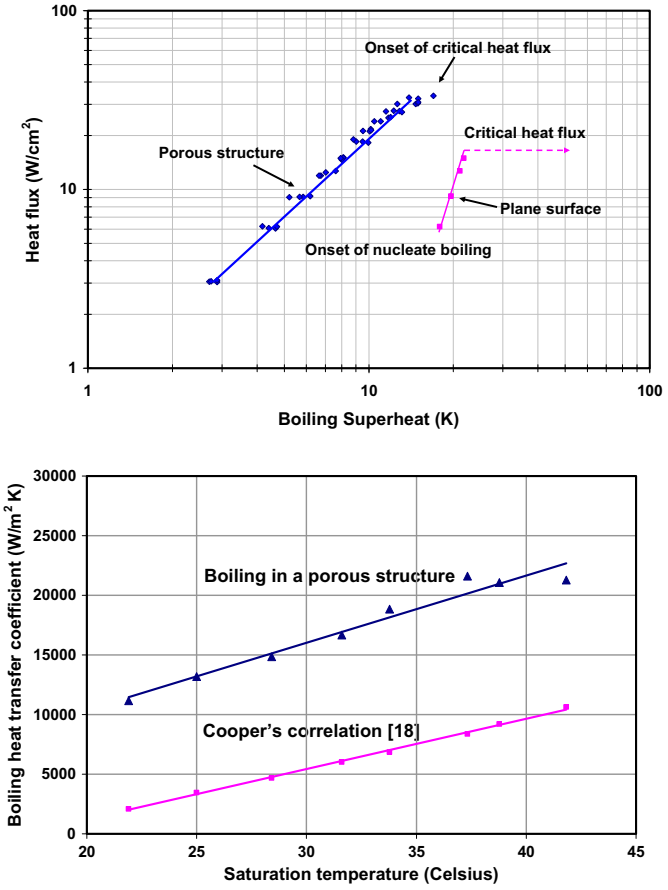

Fig. 8. (a) Boiling curves of porous surface and plane surface at sub-atmospheric pressures. (b) Boiling heat transfer coefficients at various saturation temperatures.

more active nucleation sites are observed with higher bubble-departure frequency of one bubble per 50–60 ms. It is clear from these figures that bubble detachment occurs only when two nearby bubbles coalesce, forming a larger bubble that has greater buoyancy effect. To sustain such phenomenon, a higher wall superheat is needed for the bubble coalesce and depart. All these are mainly the contributing factors to the deterioration of boiling heat transfer coefficient at sub-atmospheric pressure.

At heat loads of 120–220 W, thermal resistances in the device can be broken down into the following; convection resistance is 0.128 K/W, boiling resistance is 0.074 K/W, condensation resistance is 0.0037 K/W, and an interface resistance of 0.054 K/W. It also shows that the heat transfer "bottleneck" within the device is the air convection from the fins contributing 50% of the total thermal resistance, while boiling, interface, and condensation resistances are only 28%, 21%, 1%, respectively. The overall device thermal resistance (without interface effect) up to 220 W cooling is only 0.206 K/W.

Classical plots of heat flux versus ΔT for the porous structure and the plane surface at sub-atmospheric pressures (2–4 kPa) are also shown in Fig. 8a. The porous structure's boiling curve being situated at a lower superheat region signifies a better boiling heat transfer performance compared to plane surface. It also shows a gradual increase unlike the steeper slope seen for plane surface, implying that there is a decrease in the boiling performance for the porous structure at higher heat fluxes caused by a vapor or bubble blob-locked inside. It prevents any liquid entry into the porous surface, showing early signs of transition to the Leidenfrost phenomena. Although no distinct critical heat flux (CHF) behavior for the porous structure is observed for the whole test. Notably, the surface heat flux has reached twice of that for a plane surface. The onset of nucleate boiling, on the other hand, started earlier (lower ΔT) with the use of porous structure as it provides a vast number of nucleation sites.

The boiling heat transfer coefficient of the porous structure is compared with a plane surface boiling predicted by the Cooper's boiling correlation [18] under reduced pressures, shown in Fig. 8b. From the lowest to the highest saturation temperature the heat flux is in the range of 3–24 W/cm^2 with a step increase of 3 W/cm^2. Both heat transfer coefficients are increasing at higher heat fluxes and saturation pressures. Significant improvement in boiling is observed with the use of the porous structure; the heat transfer coefficient is enhanced by two to four folds as compared to plane surface at low saturation temperatures, typically around 11 kW/m^2 K.

Details of air cooling is depicted by Fig. 9a which shows the different fan curves at various fan speed settings of an axial flow fan (92 mm × 25 mm) from ADDA Corp [19]. The actual and predicted air pressure drops are in close agreement with maximum deviation of only 7%. From Fig. 9b, predicted and actual convection thermal resistances are observed to have a similar trend as both gradually decrease with increased air flow rate, having a maximum percentage difference of 20%.

Orientation effects of the device are also studied. Testing rig was tilted horizontally (90° tilt) to emulate the usage inside a computer casing, and verifying whether there is performance deterioration from such positions. One aspect of two-phase closed/loop design is that it requires a vapor path to the condenser and the

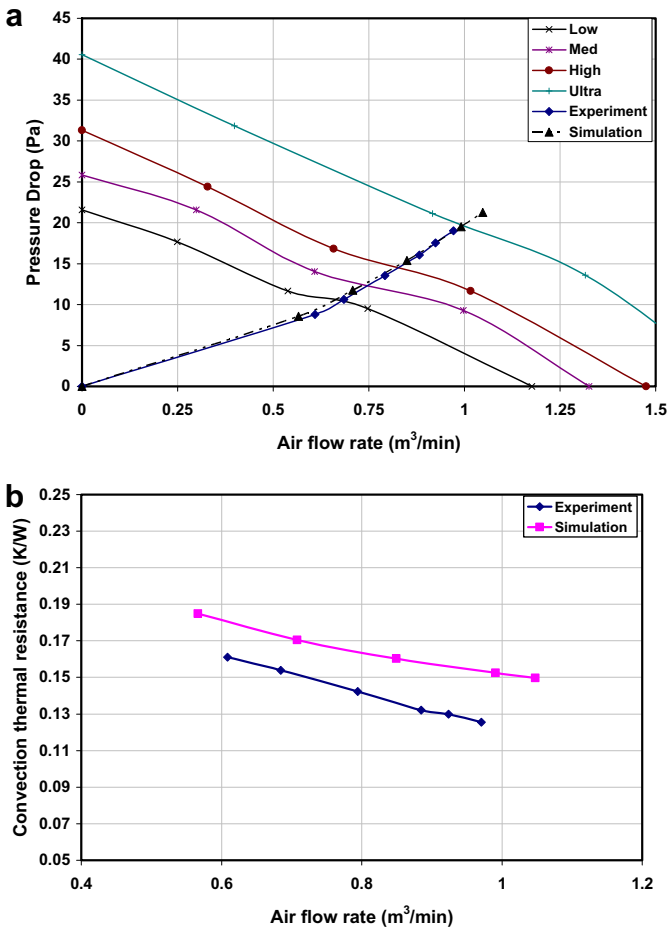

Fig. 9. (a) Air pressure drop through the cooler at various flow rates. (b) Convection thermal resistance of the curvilinear fin array at various air flow rates.

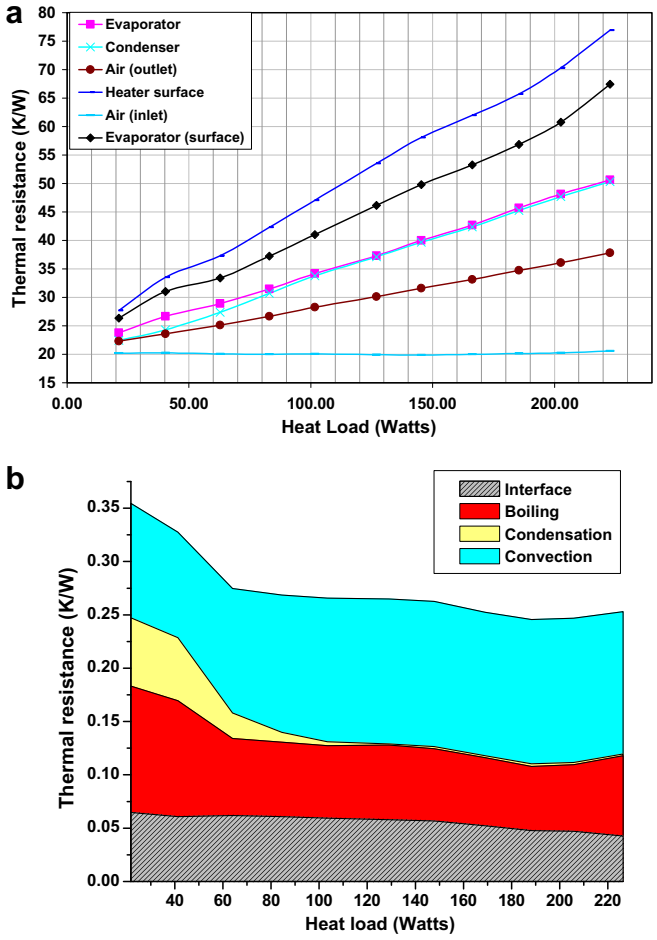

Fig. 10. (a) Steady state temperature levels at various heat loads (horizontal orientation). (b) Thermal resistances at various heat loads (horizontal orientation).

liquid condensate to flow back into the evaporator in the titled orientations. Fig. 10a shows the steady temperature readings on different parts of the device. The heater surface temperature was below 70 °C at 200 W on a slightly higher air flowrate of 1.025 m^3/min (36.2 cfm). The reason behind this improvement can be seen on both Figs. 10b and 11. With increasing heating load there is a reduction by 15.4% in the boiling resistance from 0.074 K/W to 0.0625 K/W. The horizontal orientation is observed to function well: the device permits the porous structure to be fully wetted and this allows a continuous capillary feed of working fluid to the evaporator base.

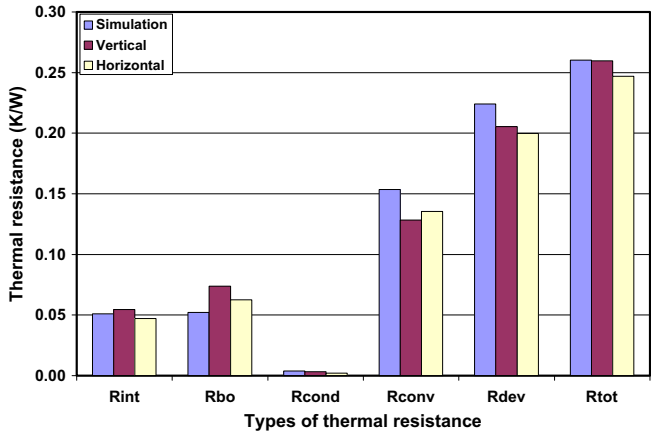

Fig. 11. Contrasts between predicted and experimental results.

Table 2
Comparison of various CPU cooling devices.

Description	Volume (cm^3)	Overall dimension height × width (mm)	Total thermal resistance (K/W)	T_o (°C)	Q_{max} (W)
Thermosyhpon (Al) [20]	463.5	184 × 97	0.175	26	100
Thermosyphon (Cu) [20]	382.7	184 × 54	0.288	24	100
Thermosyphon [21]	532.2	194 × 100	0.220	24	170
Thermosyphon [21]	904.5	194 × 200	0.185	24	190
Miniature heat pipe [4]	252.7	80 × 80	0.410	N/A	70
Loop heat pipe [5]	114.9	60 × 65	0.580	22	140
Flat loop heat pipe [6]	108.3	60 × 80	1.200	24	70
Fin-fan hear sink [1]	373.6	50 × 80	0.338	35	103
Micro-channel liquid cooling [22]	809.0	160 × 60	0.23	20	105
Author's test unit [7]	485.0	65 × 96	0.260	20	200

A summary of the different types of thermal resistance in the device under 200 W of heat load and fan flow rate of 0.98 m^3/min is shown in Fig. 11. Modeling results are compared with the experiments, showing good agreement with one another. Simulated boiling resistance tend to be underestimated, as it ignored the conductivity of the porous structure's bonding material (silver loaded epoxy) to the device's base plate. The convection resistance is overestimated by 19.66%; it is lower due to the additional surface area of the evaporator–condenser section exposed to the air stream. The total thermal resistance of the device (inclusive of interface) at vertical orientation is 0.26 K/W and slightly improved to 0.247 K/W at horizontal orientation (90° tilt).

Among the various cooling devices reviewed (shown in Table 2), the performance of this compact two-phase cooler is found to be the best as it has the most compact configuration at 200 W heating load, the total thermal resistance of the device is only 0.26 K/W.

6. Conclusion

A compact and efficient cooling device has been studied that has a cooling capacity of 220 W while maintaining the heat source temperature below the thermal design limit for normal and tilted orientations. The prototype device solved the thermal "bottleneck" of the air side convection thermal resistance contributing up to 50% of the total thermal resistance. Significant improvements could be achieved by having an optimal number of thinner curvilinear fins, providing adequate air flow and maximizing the heat transfer area on a small volumetric space. The experiment is backed up by the proprietary simulation code and thus giving us confidence for further evaluation. The proposed cooling device has out-performed cooling devices of similar size and even matching that of much larger cooling devices. It has a minimal device thermal resistance of 0.206 K/W and 0.20 K/W at 0 and 90° tilt, respectively.

References

[1] M. Siani, R.L. Webb, Heat rejection limits of air cooled plane fin heat sinks for computer cooling, IEEE Trans. Components Pack. Technol. 26 (1) (2003) 71–79.
[2] J.Y. Chang, H.S. Park, J.I. Jo, S. Julia, A system design of liquid cooling computer based on the micro cooling technology, in: 10th Intersociety Conference on Thermal and Thermomechanical Phenomena in Electronics Systems, 2006, pp. 157–160.
[3] S.H. Moon, H.G. Yun, G. Hwang, T.G. Choy, Experimental study on the performance of miniature heat pipes with woven-wire wick, IEEE Trans. Components Pack. 24 (4) (2001) 591–595.
[4] K.S. Kim, M.H. Won, J.W. Kim, B.J. Back, Heat pipe cooling technology for desktop PC CPU, Appl. Therm. Eng. 23 (1) (2003) 1137–1144.

[5] Y.F. Maydanik, S.V. Vershinin, M.A. Korukov, J.M. Ochterbeck, Miniature loop heat pipes – a promising means for cooling electronics, IEEE Trans. Components Pack. 28 (2) (2005) 290–296.
[6] R. Singh, A. Akbarzadeh, M. Mochizuki, R.R. Riehl, Miniature loop heat pipe with flat evaporator for cooling computer CPU, IEEE Trans. Components Pack. Technol. 30 (1) (2007) 42–49.
[7] K.C. Ng, C.R. Yap, M.A. Chan, I.I. El-Sharkawy, A method and apparatus for intense heat surfaces cooling to atmospheric air: a fully-integrated and evaporative-based cooling apparatus, US Provisional Patent Application No. 60/914,410, 2007.
[8] S. Lee, S. Song, V. Au, K.P. Moran, Constriction/spreading resistance model for electronic packaging, in: Proceedings of 4th ASME/JSME Thermal Engineering Joint Conference, 1995, pp. 199–206.
[9] K.C. Ng, A. Chakraborty, M.A. Sai, X. Wang, New pool boiling data for water with copper-foam metal at sub-atmospheric pressures: experiments and correlation, Appl. Therm. Eng. 26 (1) (2006) 1286–1290.
[10] W. Nusselt, Die Oberflachenkondensation des Wasserdamfes, VDI Z 60 (1) (1916) 541.
[11] J.P. Holman, Heat Transfer, eighth ed., McGraw-Hill, 1999. p. 520.
[12] R.K. Shah, A.L. London, Laminar flow forced convection in ducts, Advances in Heat Transfer, Academic Press, 1988 (Supplement 1).
[13] I.E. Idelchik, Handbook of Hydraulic Resistance, third ed., CRC Press, 1994. p. 149.
[14] D. Copeland, Optimization of parallel plate heatsinks for forced convection, in: Sixteenth IEEE SEMI-THERM Symposium, 2000, pp. 266–272.
[15] W.M. Kays, A.L. London, Compact Heat Exchangers, third ed., McGraw-Hill, 1984. p. 109.
[16] W.R. McGillis, J.S. Fitch, W.R. Hamburgen, V.P. Carey, Pool boiling enhancement techniques for water at low pressure, WRL Research Report 90/9, 1990.
[17] D. Gorenflo, Pool Boiling in VDI-Heat Atlas, VDI-Verlag, Dusseldorf, Germany, 1993 (English Version).
[18] M.G. Cooper, Saturation and nucleate pool boiling – a simple correlation, Inst. Chem. Eng. Symp. Ser. 86 (2) (1984) 785–793.
[19] ADDA Corp., Fan curve of 92 × 25 mm axial fan, 2006. Available from: <http://www.addausa.com/curves/curve_index.htm>.
[20] P.E. Tuma, H.R. Mortazavi, Indirect thermosyphons for cooling electronic devices, Electronics Cooling 12 (1) (2006) 26–32.
[21] R.L. Webb, S. Yamauchi, Test results on a thermo-syphon concept to high-power cool desktop computers and servers, in: 18th IEEE SEMI-THERM Symposium, 2002, pp. 151–158.
[22] J.Y. Chang, H.S. Park, J.I. Jo, S. Julia, A system design of liquid cooling computer based on the micro cooling technology, in: Tenth Intersociety Conference on Thermal and Thermomechanical Phenomena and Emerging Technologies in Electronic Systems, IEEE, San Diego, CA, 2006, pp. 157–160.